Particle & Particle Systems Characterization
www.particle-journal.com

High-Temperature Stable Zirconia Particles Doped with Yttrium, Lanthanum, and Gadolinium

*Elisabeth W. Leib, Robert M. Pasquarelli, Malte Blankenburg, Martin Müller, Andreas Schreyer, Rolf Janssen, Horst Weller, and Tobias Vossmeyer**

Zirconia microspheres synthesized by a wet-chemical sol–gel process are promising building blocks for various photonic applications considered for heat management and energy systems, including highly efficient reflective thermal barrier coatings and absorbers/emitters used in thermophotovoltaic systems. As previously shown, pure zirconia microparticles deteriorate at working temperatures of ≥1000 °C. While the addition of yttrium as a dopant has been shown to improve their phase stability, pronounced grain growth at temperatures of ≥1000 °C compromises the photonic structure of the assembled microspheres. Here, a new approach for the fabrication of highly stable ceramic microparticles by doping with lanthanum, gadolinium, and a combination of those with yttrium is introduced. The morphological changes of the particles are monitored by scanning electron microscopy, ex situ X-ray diffraction (XRD), and in situ high-energy XRD as a function of dopant concentration up to 1500 °C. While the addition of lanthanum or gadolinium has a strong grain growth attenuating effect, it alone is insufficient to avoid a destructive tetragonal-to-monoclinic phase transformation occurring after heating to >850 °C. However, combining lanthanum or gadolinium with yttrium leads to particles with both efficient phase stabilization and attenuated grain growth. Thus, ceramic microspheres are yielded that remain extremely stable after heating to 1200 °C.

1. Introduction

Zirconium dioxide is a versatile material with excellent mechanical properties,[1] high refractive index and low thermal conductivity[2] and it has numerous applications in ceramics and catalysis.[3] Moreover, well-defined zirconia microparticles with narrow size distributions are gaining ever increasing interest as building blocks for novel photonic materials suited for high-temperature applications, such as advanced reflective thermal barrier coatings (TBCs)[4–6] and as absorbers/emitters in thermophotovoltaics.[7] However, their use in high-temperature applications is limited due to a martensitic phase transformation that the material undergoes upon cooling below 1170 °C and which is accompanied by a volume expansion of ≈4%, which subsequently leads to material failure.[8] This destructive transformation from the metastable tetragonal phase (P42/nmc) to the thermodynamically stable monoclinic phase (P21/c) can be avoided by stabilizing the material in either the tetragonal or the more symmetric cubic phase (Fm3m). This stabilization is achieved by doping the material with aliovalent cations, most commonly with yttrium.[9–12] Yttria-stabilized zirconia (YSZ) has a high chemical and thermal stability and is widely used in fuel cells[13] and in high-temperature applications, such as TBCs.[14] TBCs are used to reduce the heat load on components in gas turbines. Improving the TBC performance would enable either higher operating temperatures (and thus efficiencies) or extend the turbine lifetime. A temperature decrease of only 13 °C leads to a doubling of the turbine blade lifetime.[15] Materials used in TBCs should have a high melting point, low thermal conductivity and chemical inertness, exhibit no phase transformations between room and working temperature, and are currently limited to working temperatures of ≤1250 °C.[14]

Previously, we have proposed a novel highly reflective film as the basis for the development of a new kind of TBC. The film consisted of a photonic glass assembled from ceramic microspheres with a broadband reflection in the infrared spectrum.[6] This approach allows for an enhanced reduction of heat input into the material by taking advantage of its photonic properties to reflect undesirable thermal radiation and thus achieve a higher thermal stability and better protection of the component. Recently, we reported on the synthesis of yttria-stabilized microspheres as building blocks for such a reflective coating and assessed the performance of assembled photonic glass films after heating to temperatures of up to 1400 °C.[16] From this

E. W. Leib, Prof. H. Weller, Dr. T. Vossmeyer
University of Hamburg
Institute of Physical Chemistry
Grindelallee 117, 20146 Hamburg, Germany
E-mail: tobias.vossmeyer@chemie.uni-hamburg.de
Dr. R. M. Pasquarelli, Dr. R. Janssen
Hamburg University of Technology
Institute of Advanced Ceramics
Denickestraße 15, 21073 Hamburg, Germany
M. Blankenburg, Prof. M. Müller, Prof. A. Schreyer
Helmholtz-Zentrum Geesthacht
Institute of Materials Research
Max-Planck-Straße 1, 21502 Geesthacht, Germany

The copyright line was updated 14 July 2016 after initial publication.

This is an open access article under the terms of the Creative Commons Attribution-NonCommercial License, which permits use, distribution and reproduction in any medium, provided the original work is properly cited and is not used for commercial purposes.

DOI: 10.1002/ppsc.201600069

work, it was found that while phase stabilization was achieved, grain growth within and sintering between assembled particle networks remain a current challenge at temperatures above 1200 °C. While Y-doping was found to reduce grain growth, its contribution alone was not sufficient for the desired microstructural stabilization. As such, alternative doping strategies must be explored to reduce heat-driven diffusion processes and grain boundary mobility more efficiently.

Doping zirconia with rare-earth elements has been shown to lower grain boundary mobility by (1) decreasing the interfacial energy and thereby the driving forces for growth and by (2) increasing the activation energy for boundary diffusion. The latter is a consequence of solute segregation and increased solute drag.[17–19] In general, dopants of lower valence and larger ionic radii than Zr^{4+} are correlated with smaller grain sizes and less growth. For bulk zirconia, La-doping has been correlated with an increased activation energy for grain growth and thus reduced grain growth rates.[13] Especially, a combination of La with YSZ was found to increase thermal stability.[20] Gd-doping has also previously been shown to decrease grain growth in bulk zirconia.[17] However, to our knowledge, the introduction of La and Gd and their combination with Y into micrometer-sized, spherical particles and their effects on phase stability, grain growth, and particle shape persistency have not been studied previously.

At higher solute concentrations, rare-earth elements can form compounds with zirconia, crystallizing in the pyrochlore structure ($A_2B_2O_7$).[21–24] $La_2Zr_2O_7$ and $Gd_2Zr_2O_7$ have been considered for TBC applications due to their high melting points, phase stabilities, and low thermal conductivities. However, their use is impeded by a low toughness compared to YSZ[25] and a thermal expansion mismatch between the coating and metallic layer in the components.[14] For this reason, mixed-phase layers and double layers of YSZ and pyrochlores have been proposed for TBC applications as strategies to combine the thermal and mechanical stabilities of each system.[25,26]

In this work, we employed a sol–gel approach to synthesize La- and Gd-doped microparticles with diameters in the 2–3 µm range and size standard deviations as low as 4.7%. The dopant molar contents were varied from 0.5% to 3%. The particles were examined with respect to phase transformations, grain growth, and particle disintegration as a function of temperature up to 1500 °C using X-ray diffraction (XRD) and scanning electron microscopy (SEM). The dopant content in the particles was analyzed via inductively coupled plasma optical emission spectroscopy (ICP-OES). Furthermore, codoping with Y for phase stabilization and with La/Gd for additional grain growth control was also explored.

2. Results and Discussion

2.1. Particle Synthesis

Zirconia particles doped with La, Gd, and a combination of those with Y were obtained through a modified sol–gel wet chemical process, which was previously introduced by our group for the synthesis of Y-doped and undoped zirconia particles.[16,27] The method is based on the approach initially introduced by Yan et al.[28,29] Monodoped particles were synthesized with La/(La+Zr) and Gd/(Gd+Zr) molar ratios of 0.5%, 1.0%, 1.5%, 2.0%, and 3.0%. In the following, these samples will be referred to as La0.5, La1.0, La1.5, La2.0, La3.0 and Gd0.5, Gd1.0, Gd1.5, Gd2.0, Gd3.0, respectively. Codoped particles with Y ratios of 5% and La or Gd ratios of 1% were also synthesized and are hereafter referred to as YLa and YGd. As shown for representative samples La1.0, Gd1.0, YLa, and YGd in **Figure 1**, all as-synthesized particles were spherical and displayed varying degrees of smoothness, the cause of which is not clear at this point. SEM images of all particle samples can be found in the Supporting Information (Figures S2 and S3). Typically, their diameters were in the 2–3 µm range. Particle sizes, standard deviations, and the particle size spans (as given by (x90-x10)/x50) are listed in **Table 1**.

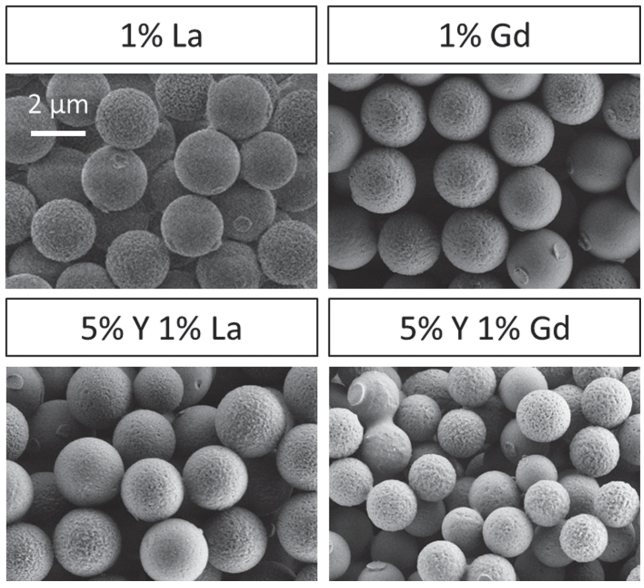

Figure 1. Representative SEM images of as-synthesized samples La1.0, Gd1.0, YLa, and YGd. The scale bar applies to all images. SEM images of all samples synthesized in this study can be found in the Supporting Information (Figures S2 and S3).

For both the La- and Gd-doped particles, it was observed that an increase in dopant concentration had no pronounced effect on the size distributions of the particles, with an average size standard deviation of 5.6% and a variance of only 0.8%. Only sample La3.0 exhibited a larger size distribution of 10.7%, but this may be due to variations between syntheses and thus the sample was excluded from the prior statistical analysis. This behavior is in contrast to previous observations for Y-doped zirconia microparticles, which exhibited both broader size distributions and a trend of broadening size distributions with an increasing amount of added dopant precursor.[16] Heating of the as-synthesized samples resulted in a considerable mass loss and shrinkage of the particles. In accordance with our previous study,[27] the main mass loss event, as determined by TGA, occurred with heating to 450 °C and resulted in a decrease in the particle diameters of ≈30%. Heating to higher temperatures did not cause any further shrinkage. Particle diameters as a function of heating temperature are shown in the Supporting Information for samples La1.0, Gd1.0, YLa, and YGd (Figure S6). Moreover, particle shrinkage had virtually no influence on the particle size distributions. Size distributions for

© 2016 The Authors. Published by WILEY-VCH Verlag GmbH & Co. KGaA, Weinheim

Table 1. Diameters of as-synthesized particles (before heat treatment), size standard deviations and spans, and differences in dopant contents between target and ICP-OES measured values for monodoped and codoped microparticles.

	Diameter as-synthesized [nm]	Size standard deviation [%]	Span (x90-x10)/x50 [–]	Target dopant content [%]	Found(ICP-OES) [%]	Difference [relative%]
La0.5	2420	5.6	9.3	0.5	0.45	–10%
La1.0	2235	6.9	12.7	0.99	0.78	–21%
La1.5	2525	5.5	9.0	1.51	1.26	–17%
La2.0	2495	6.0	12.2	2.07	1.63	–21%
La3.0	2027	10.7	25.8	3.06	2.41	–21%
Gd0.5	2725	6.9	11.6	0.52	0.50	–3.8%
Gd1.0	2384	6.2	11.3	1.02	1.10	+7.8%
Gd1.5	2336	4.7	9.6	1.50	1.56	+4.0%
Gd2.0	2348	6.0	13.8	2.00	1.97	–1.5%
Gd3.0	3047	4.8	11.2	2.99	2.95	–1.3%
YLa	2338	6.5	12.6	4.97/0.98	6.03/0.77	+21%/ – 21%
YGd	1859	7.2	12.9	4.98/1.06	6.51/1.35	+31%/ + 27%

samples YLa and YGd as a function of heating temperature are represented in the Supporting Information (Figure S7).

The elemental composition of the particles was examined via ICP-OES. A comparison of the target and the measured dopant concentrations is shown in Table 1. In the case of La-doping, the measured dopant content was consistently lower (by between 10–21 relative%) than the target dopant content calculated from the amount of added precursors. This is in contrast to the Gd-doped particles, where the measured dopant concentrations were in much better agreement with the target concentrations (deviation between –3.8 and +7.8 relative%). This difference in behavior was also confirmed for the codoped samples YLa and YGd, where the measured Y and Gd contents were higher and the measured La content was lower than the target compositions. All deviations of the measured values from the target values were significantly larger than the precision between ICP replicates (0.5–1 relative% for La and 0.1–0.4 relative% for Gd), indicating that the difference of incorporation between dopants is genuine. For samples YLa and YGd, SEM-EDX mapping showed no indication of an inhomogeneous distribution of the dopants within the particles (Supporting Information Figures S22 and S23).

Considering that all synthetic parameters (content of educts, duration, and temperature of the reaction) were identical and all three dopants were introduced to the reaction in the form of *iso*-propoxides, the only differences between Y, La, and Gd reside in their ionic radii (Y: 104 pm, La: 117 pm, Gd: 108 pm)[30] and their electronegativities (Y: 1.22, La: 1.10, Gd: 1.20). Both parameters are nearly identical for Y and Gd, while La displays a comparatively greater deviation. Hence, La differentiates most from the host Zr ion (ionic radius of 84 pm[30] and electronegativity of 1.33), and this may account for its lower degree of incorporation. Alternatively, it is possible that this effect is not related to the intrinsic properties of the ions but rather the structural properties of the *iso*-propoxides. Alkoxides of Ti, Zr, and lanthanide-series elements are known to form polynuclear clusters with various degrees of coordination. The propensity of one structure over another to undergo hydrolysis and condensation may account for the differences in incorporation observed.[31,32]

2.2. Stability of La-Doped Microparticles

The influence of the introduction of dopants on the zirconia particles' high-temperature stability was first assessed by ex situ characterization after heat treatments at temperatures of up to 1500 °C. The employed heating profiles can be found in the Supporting Information (Figure S1). The morphology and stability of the particles were examined by taking SEM images of deposits from suspensions, which were obtained by sonicating the calcined particles in ethanol. Additionally, the internal structure and sintering processes of the particles were evaluated via XRD measurements by analyzing their crystalline phases and grain sizes as a function of heating temperature.

Figure 2a shows SEM images of particle samples doped with 0.5%, 1.0%, 1.5%, 2.0%, and 3.0% La after heating at 1200 °C for 3 h. Samples La0.5 and La1.0 consisted of stable, spherical particles with a rough surface and visible grains. The particles in sample La1.5 showed a roughened morphology with larger grains and some particle disintegration. More pronounced disintegration was observed for samples La2.0 and La3.0, where only few particles remained intact. Hence, above a dopant concentration of 1.0%, the particle stability decreased with increasing La content.

The retained room temperature phases of the La-doped samples are shown in **Table 2**. A complete series of X-ray diffractograms for all La-doped samples at all examined temperatures can be found in the Supporting Information (Figures S8–S12). Particles heated at 250 °C were initially amorphous and crystallized to the tetragonal phase after heating to 450 °C. Heating at higher temperatures resulted in a transformation to the monoclinic phase, which was shifted to higher temperatures with increasing La contents. Thus, the tetragonal-to-monoclinic transformation took place after heating to 850 °C for La0.5, to 1000 °C for samples La1.0 and La1.5, and only after heating to 1200 °C for samples La2.0 and La3.0. At high La concentrations of 2.0% and 3.0%, a pyrochlore $La_2Zr_2O_7$ phase also formed alongside the monoclinic phase after heating to 1200 °C (shown in Figure 2c). These results are consistent with the

 © 2016 The Authors. Published by WILEY-VCH Verlag GmbH & Co. KGaA, Weinheim

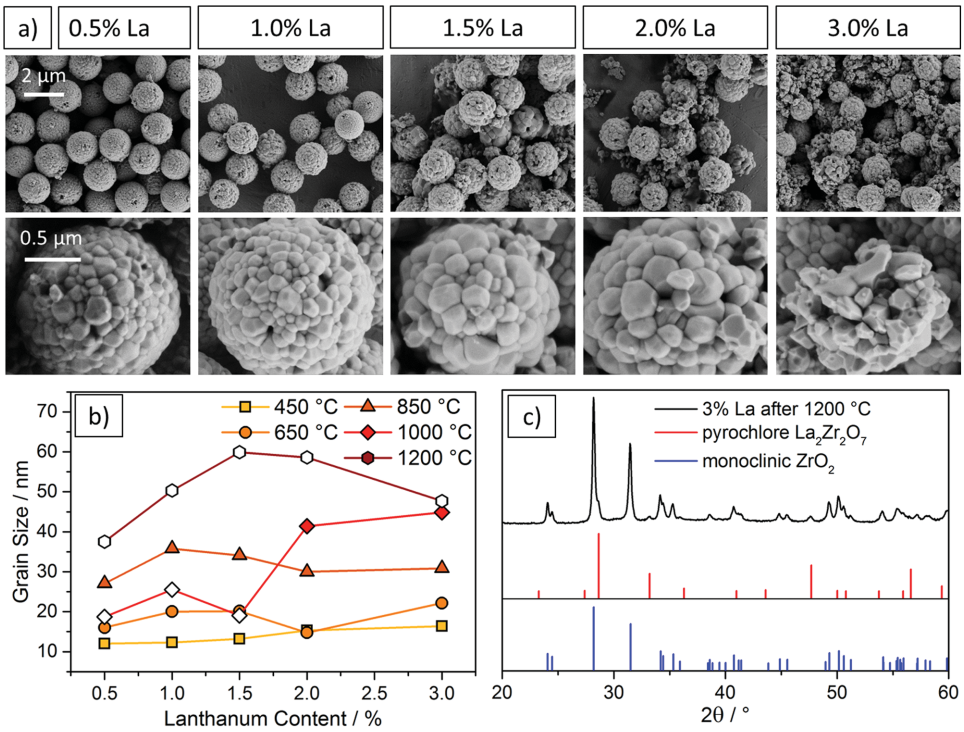

Figure 2. a) SEM images of zirconia particles doped with 0.5%, 1.0%, 1.5%, 2.0%, and 3.0% La after heating at 1200 °C for 3 h. Samples are shown at low magnification (top row) and high magnification (bottom row). Scale bars apply to all images within a row. b) Grain sizes of La-doped particles as a function of La content after heating to temperatures of 450, 650, 850, 1000, and 1200 °C. Grain sizes were obtained from X-ray diffraction measurements, using the Scherrer equation. Filled-in symbols represent the tetragonal phase, open symbols the monoclinic phase. c) Powder X-ray diffraction patterns of sample La3.0 after heating to 1200 °C showing reflexes of pyrochlore $La_2Zr_2O_7$ (red) and monoclinic ZrO_2 (blue).

findings of Bastide et al. for La-doped bulk zirconia, for which both a stabilization of the tetragonal phase with increasing La content and the formation of a pyrochlore phase after heating to 1200 °C were documented.[21] Furthermore, the appearance of the pyrochlore phase coincided with the observed increase in particle disintegration at high dopant concentrations. This finding can possibly be attributed to a mismatch in thermal expansion coefficient between $La_2Zr_2O_7$ (9.1–9.7 × 10^{-6} K^{-1}) and ZrO_2/YSZ (10.3 × 10^{-6} K^{-1}, 10.5–11.5 × 10^{-6} K^{-1}).[5,14] After further heating to 1500 °C, all samples displayed texturing of the monoclinic phase with respect to the (002) reflex. Additionally, the pyrochlore phase was no longer observed for samples La2.0 and La3.0. The pyrochlore phase is likely a result of segregation and enrichment of La at the grain boundaries due to

Table 2. Retained room temperature phases of samples doped with La, Gd, and Y after heating to various temperatures for 3 h at each temperature with a = amorphous, t = tetragonal, m = monoclinic, and py = pyrochlore structures. Phases detected in trace amounts shown in parentheses.

	250 °C	450 °C	650 °C	850 °C	1000 °C	1200 °C	1500 °C[a)]
La0.5	a	t	t + (m)	t + m	m	m	m
La1.0	a	t	t	t	m + (t)	m	m
La1.5	a	t	t	t	m + t	m	m
La2.0	a	t	t	t	t + (m)	m + (py)	m
La3.0	a	t	t	t	t + (m)	m + py	m
Gd0.5	a	t	t	m + t	m	m	m
Gd1.0	a	t	t	t + (m)	m + (t)	m	m
Gd1.5	a	t	t	t	m + (t)	m	m
Gd2.0	a	t	t	t	m + t	m	m
Gd3.0	a	t	t	t	t	m + (t)	m + py
YLa	a	t	t	t	t	t	t + (m)
YGd	a	t	t	t	t	t	t

[a)]All La- and Gd-monodoped samples textured with respect to the (002) reflex after heating at 1500 °C.

© 2016 The Authors. Published by WILEY-VCH Verlag GmbH & Co. KGaA, Weinheim

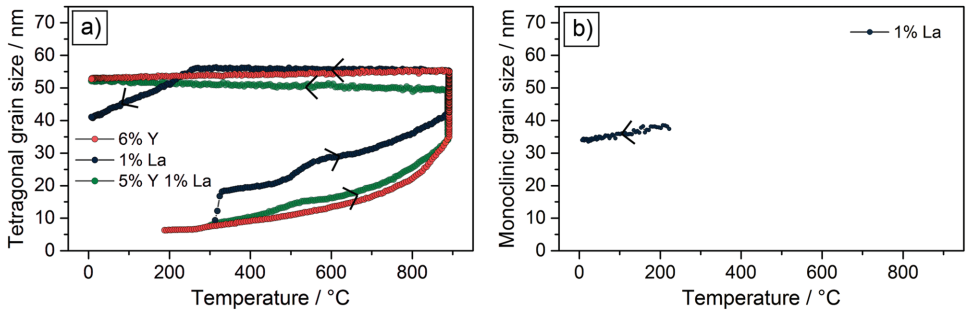

Figure 3. a) Tetragonal crystallite sizes for samples La1.0, YLa, and a YSZ sample with a Y content of 6%. b) Monoclinic crystallite sizes for sample La1.0. All samples were heated to a maximum temperature of ≈900 °C and held for 60 min. The heating and cooling rates were ≈11 °C min^{-1}. Arrows indicate direction of heating and cooling.

space-charge driving forces[19] and/or solute drag during grain growth. At 1500 °C, mass transport is sufficiently high to allow for the phase to go into solid solution with the zirconia. This was confirmed with secondary heating experiments in which particles that formed $La_2Zr_2O_7$ as a second phase at 1200 °C were reheated at 1500 °C. The diffraction reflexes for $La_2Zr_2O_7$ were no longer observed after reheating (see Supporting Information Figure S20), suggesting redissolution of the $La_2Zr_2O_7$ into the monoclinic phase. The La concentrations for the particles (3% and less) are borderline with the range for solid solubility in monoclinic zirconia, as given by the phase diagrams for the La_2O_3-ZrO_2 system,[22–24] but are higher than maximum solubility of 1% La reported by Bastide et al.[21] Lastly, after heating at 1500 °C, all samples were fully sintered and had lost their spherical shape, as shown in the Supporting Information (Figure S4).

The grain sizes of the La-doped particles were determined with the Scherrer equation from XRD measurements as a function of temperature and are shown in Figure 2b. Four regimes were identified. In the first, the initial grain sizes of La-doped particles heated to 450 °C were found to slightly increase with an increasing La content (from 12 to 16 nm). The second regime was characterized by the retention of the tetragonal phase. This corresponds to 650 and 850 °C for all examined compositions and to 1000 °C for La2.0 and La3.0. For a fixed composition, it was observed that an increase in heating temperature of 200 °C corresponded to an increase in grain size of ≈10–15 nm. For a fixed temperature, no obvious trend was discerned as a function of composition. After heating to 650 and 850 °C, the grain sizes first increased from 0.5% to 1.0% La, then decreased over 1.5% La to 2.0% La, and lastly increased again for a La content of 3.0%.

The third regime corresponded to the samples after heating to 1000 °C at which La0.5, La1.0, and La1.5 had already transitioned to the monoclinic phase, as opposed to samples La2.0 and La3.0 which remained tetragonal. The monoclinic grains of samples La0.5, La1.0, and La1.5 were relatively small (18–26 nm), even below the tetragonal grain sizes of those samples heated to the lower temperature of 850 °C (26–36 nm). Notably, the measured grain sizes after the phase transformation at 1000 °C were smaller than before it at 850 °C.

High-energy XRD (HE-XRD) measurements were performed in situ during heating and cooling to identify the mechanism for the observed grain size reduction. **Figure 3** shows the tetragonal and monoclinic grain sizes measured in samples La1.0, YLa and a pure YSZ sample with a Y content of 6% for comparison.[16] The three samples were heated in situ to a maximum temperature of ≈900 °C, held at this temperature for 60 min, and then cooled, using rates of 11 °C min^{-1}. In all three samples, initial crystallization into the tetragonal phase occurred at 200–300 °C. The tetragonal grains then grew with increasing temperature and during the hold, reaching sizes up to 50–55 nm. For the YSZ particles, the grain sizes remained more or less constant upon cooling and no phase transformation was observed. However, sample La1.0 exhibited a decrease in the tetragonal grain size from 55 to 40 nm upon cooling below a critical transformation temperature of ≈250 °C. More importantly, the final monoclinic grain sizes (≈35 nm) were 30%–36% smaller than their parent tetragonal grains from which they transformed (50–55 nm). This behavior was observed at both higher heating/cooling rates (90 °C min^{-1}) and for higher holding temperatures (see Supporting Information Figure S21), with 1200 °C resulting in ≈150 nm tetragonal grains transforming into ≈50 nm monoclinic grains. Interestingly, it contrasts in situ measurements of undoped zirconia particles, for which the transformed monoclinic grains retained a similar grain size as their parent tetragonal grains.[27] Thus, it appears that La-doping alters the transformation mechanism from a one-to-one, tetragonal-to-monoclinic process into one in which smaller monoclinic grains form within larger initial tetragonal grains. The overall process is schematically represented in **Figure 4**a. It is not yet clear as to whether this occurs via twinning or a nucleation process. Twinning during transformation (depicted in Figure 4b) has been observed in zirconia[33–36] and is suggested to occur in order to relieve stresses. Alternatively, enrichment of La at the surface during grain growth may be the source. The latter is consistent with simulations and experimental results reported by Wang et al. on mixed YSZ-$La_2Zr_2O_7$ composite coatings.[37] Wang et al. observed that the presence of $La_2Zr_2O_7$ promoted the formation of the monoclinic phase. Furthermore, the zirconia and $La_2Zr_2O_7$ grains exhibited coherent interfaces, implying that the tetragonal zirconia phase is transformed more readily where it contacts $La_2Zr_2O_7$. This supports the idea that the pyrochlore phase or La-enriched interfaces can serve as nuclei for or provide stress concentrations to induce the phase transformation and may account for the 'sub-grain' formation observed (process schematically depicted in Figure 4c).

© 2016 The Authors. Published by WILEY-VCH Verlag GmbH & Co. KGaA, Weinheim

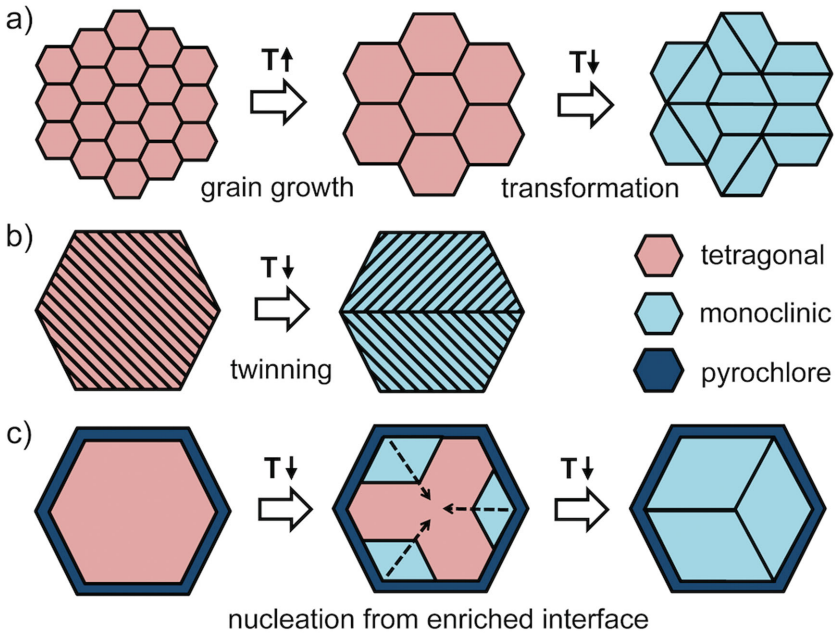

Figure 4. a) Schematic diagram depicting grain growth upon heating and formation of smaller monoclinic 'sub-grains' from within larger tetragonal grains upon cooling. Possible mechanisms of monoclinic grain formation by b) twinning and c) nucleation at interface with the pyrochlore phase or a La-enriched region.

Lastly, regime four of the ex situ grain size behavior (Figure 2b) refers to the heating experiments at 1200 °C in which all samples were monoclinic after cooling to room temperature. Overall, grain growth after heating to 1200 °C was significantly suppressed (38–60 nm as determined by HE-XRD and 50–180 nm by SEM) with La-doping compared to undoped particles (863 nm)[27] or YSZ particles (136–340 nm).[16] The grain sizes increased up to a La content of 1.5% after which they decreased. This decrease in grain size at high La contents coincided with the formation of the pyrochlore phase. If one assumes that the pyrochlore phase is formed from the segregated La ions at the grain boundaries, the phase might encapsulate the grains and act as a diffusion barrier. Second phases are known to inhibit grain boundary diffusion (also known as Zener pinning).[13]

2.3. Stability of Gd-Doped Microparticles

Similarly to the experiments conducted on La-monodoped particles, the high-temperature stability of Gd-monodoped particles was assessed via SEM and XRD measurements of samples heated up to 1500 °C. SEM-images of monodoped samples with Gd/(Gd+Zr) molar contents of 0.5%, 1.0%, 1.5%, 2.0%, and 3.0% after heating to 1200 °C are shown in **Figure 5**a. Samples Gd0.5, Gd1.0, and Gd1.5 consisted of spherical particles with roughened and granular surfaces, as well as partially and completely disintegrated particles that have broken apart. Particles in sample Gd2.0 had similarly roughened surfaces with visible grains, but the overall particle stability was higher with considerably less disintegration compared to samples Gd0.5, Gd1.0, and Gd1.5. Virtually no difference in grain sizes was observed between Gd1.0, Gd1.5, and Gd2.0. Sample Gd3.0 consisted of particles with comparatively smaller grains and showed barely any particle disintegration. This improved thermal stability with increasing Gd content was in contrast to the observations made for La-doped particles, which displayed their highest thermal stability at a low La content of 0.5%–1.0%.

In order to be able to explain the different behavior of La- and Gd-monodoped zirconia, it is important to consider the crystalline phases and microstructure of the Gd-doped particles. The retained room temperature phases of the Gd-monodoped particles are shown in Table 2 and in the Supporting Information (Figure S14–S18). A progression similar to that of the La-monodoped particles could be seen. The initially amorphous particles crystallized into the tetragonal phase after heating at 450 °C and remained that way until 650 °C. Sample Gd0.5 was predominantly monoclinic after heating to 850 °C while samples Gd1.0 to Gd3.0 remained tetragonal. After heating to 1000 °C, the monoclinic phase became dominant and only the highest doped sample Gd3.0 was still fully tetragonal. Heating to 1200 and 1500 °C caused all samples to crystallize in the monoclinic phase. After heating at 1500 °C, all particle samples were fully sintered (as shown in the Supporting Information Figure S5). Texturing was observed with respect to the (002) reflex, although it was less pronounced than in the La-monodoped samples. Furthermore, a second phase appeared after heating sample Gd3.0 to 1500 °C, which was identified to be the pyrochlore $Gd_2Zr_2O_7$ (shown in Figure 5c). This is somewhat different from the appearance of the pyrochlore $La_2Zr_2O_7$ observed in sample La3.0, which formed after heating to a lower temperature of 1200 °C but disappeared again after heating to 1500 °C. While the formation of the pyrochlore phase was correlated with a reduced stability for the La-doped particles, the fact that the $Gd_2Zr_2O_7$ phase is not yet present for the Gd-doped particles at 1200 °C may account for the differences in stability observed between La- and Gd-doped particles at this temperature. Additionally, the strain contributions due to differences of thermal expansion coefficients between the matrix and the pyrochlore phase would be less for Gd. The values are similar for ZrO_2/YSZ (10.3×10^{-6} K^{-1}, $10.5–11.5 \times 10^{-6}$ K^{-1})[5,14] and $Gd_2Zr_2O_7$ (10.4×10^{-6} K^{-1}),[26,38] in contrast to $La_2Zr_2O_7$ ($9.1–9.7 \times 10^{-6}$ K^{-1})[14] which has a greater deviation.

Grain sizes of the Gd-doped samples are represented in Figure 5b. Again, different regimes could be distinguished. In a first regime, particles heated to 450 and 650 °C retained the tetragonal phase. For a fixed sample composition, the grain size increased in all cases with increasing temperature. At a fixed temperature, a progression of grain sizes similar to that in the second regime of the La-doped particles was observed: the grain sizes first increased slightly from 0.5% to 1.0% Gd, then decreased over 1.5% Gd to 2.0% Gd, and increased slightly again for a Gd content of 3.0%. The second regime refers to

© 2016 The Authors. Published by WILEY-VCH Verlag GmbH & Co. KGaA, Weinheim

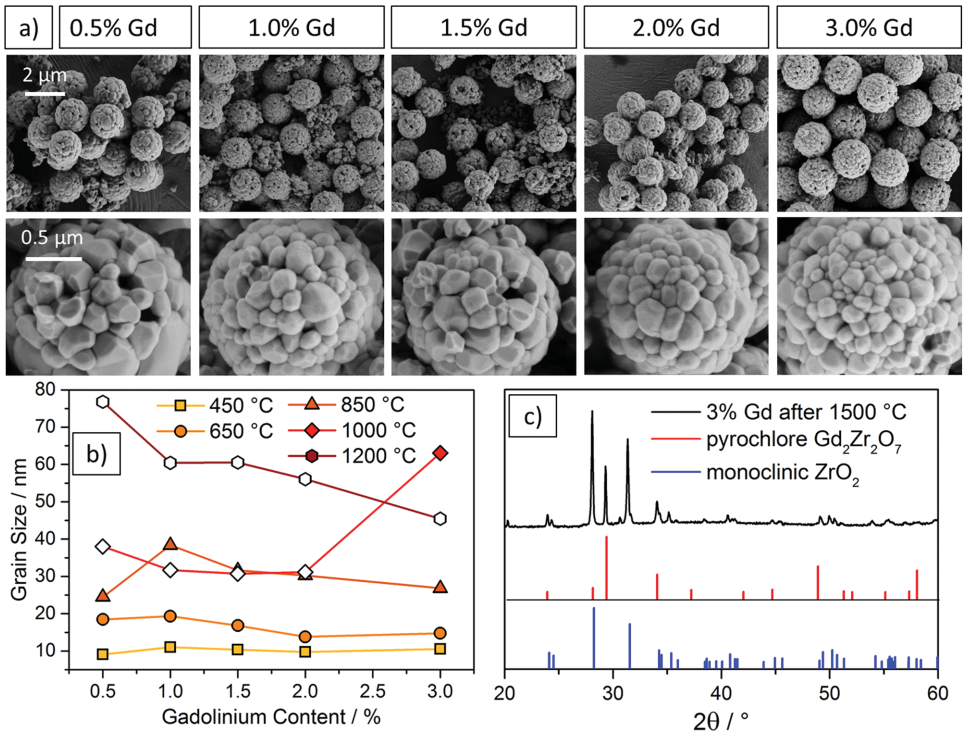

Figure 5. a) SEM images of zirconia particles doped with 0.5%, 1.0%, 1.5%, 2.0%, and 3.0% Gd after heating at 1200 °C for 3 h. Samples are shown at low magnification (top row) and high magnification (bottom row). Scale bars apply to all images within a row. b) Grain sizes of Gd-doped particles as a function of Gd content after heating to temperature of 450, 650, 850, 1000, and 1200 °C. Grain sizes were obtained from X-ray diffraction measurements, using the Scherrer equation. Filled-in symbols represent the tetragonal phase, open symbols the monoclinic phase. c) Powder X-ray diffraction patterns of sample Gd3.0 after heating to 1500 °C showing reflexes of pyrochlore $Gd_2Zr_2O_7$ (red) and monoclinic ZrO_2 (blue).

grain sizes after heating to 850 °C. A similar grain size progression with dopant content was observed (from 24 nm at Gd0.5 up to 38 nm at Gd1.0 and down to 30 nm at Gd2.0 and 27 nm at Gd3.0). The third regime, similar to the La-doped samples, describes grain sizes after heating to 1000 °C. Again, samples with lower contents from 0.5%–2.0% had transitioned to the monoclinic phase. This coincided with small grain sizes (31–38 nm). And once again, the highest doped sample, Gd3.0, remained in the tetragonal phase and displayed a comparatively high grain size (63 nm). The fourth regime consists of the samples heated to 1200 °C, which had all transitioned to the monoclinic phase. Here, the grain sizes decreased with an increasing dopant content from 77 nm for Gd0.5 to 45 nm for Gd3.0. Thus, as in the case of La-doping, Gd-doped particles heated to 1200 °C displayed a grain growth suppression when compared to both undoped particles (863 nm)[27] and YSZ particles (136–340 nm).[16] The grain size progression also confirms the earlier mentioned observation of a better stability and lower degree of particle disintegration with increasing dopant content. This is most likely related to differences in the respective pyrochlore phases, with $Gd_2Zr_2O_7$ forming only at a higher temperature of 1500 °C.

Only after heating to 1500 °C were pronounced grain growth differences between the Gd- and La-doped samples observed. SEM images can be found in the Supporting Information (Figures S4 and S5). Average grain sizes (as measured from SEM, shown in the Supporting Information Table S2) for the Gd-doped samples were smaller than those determined for the La-doped samples. Furthermore, Gd-doping still resulted in a decrease in grain size with increasing dopant concentration (1.86 to 1.02 µm from 0.5% to 3.0% Gd), while La-doping conversely produced an increase in grain size from 3.39 to 5.18 µm over the same concentration range and exhibited abnormal grain growth. At the 3.0% level, the average grain size for Gd-doped microparticles was five times smaller than for La-doped particles. Again, the results suggest Gd-doping to be the better candidate between the two.

2.4. Stability of Codoped Microparticles

In order to combine the beneficial effects of doping zirconia microparticles with La/Gd (grain growth inhibition) and Y (tetragonal or cubic phase stabilization), codoped particles with an intended Y content of 5% and La/Gd contents of 1% were fabricated. A total dopant concentration of 6% was selected based on values previously determined for YSZ microparticles.[16] A La/Gd content of 1% was selected as to avoid complications from pyrochlore formation at higher dopant concentrations at elevated temperatures. The two samples YLa and YGd consisted of fairly smooth, uniform particles with diameters of ≈2.3 and ≈1.9 µm and low size standard deviations of 6.5% and 7.2% (see Figure 1). The as-synthesized particles were amorphous and transitioned to the tetragonal phase after heating to 450 °C. The tetragonal phase was fully stabilized up to 1500 °C for sample YGd and only a small fraction

© 2016 The Authors. Published by WILEY-VCH Verlag GmbH & Co. KGaA, Weinheim

of monoclinic appeared for sample YLa after heating at 1500 °C (see Table 2 and Supporting Information Figures S13 and S19). The combined molar dopant content of 6% is lower compared to pure YSZ particles, where a full stabilization of the tetragonal phase up to 1200 °C was only achieved with a minimum of 8% Y and where stabilization at 1500 °C could only be achieved with the cubic phase using 10% Y.[16] Li et al. found that the stabilization of the tetragonal phase is more facile for La- than for Y-doping, presumably because of the larger ionic radius of La (117 pm) in comparison to Y (104 pm) and the resulting, more pronounced lattice distortion.[39] The ionic radius of Gd (108 pm) is only slightly larger than that of Y (104 pm), so in this case the good tetragonal stabilization is most likely due to the higher degree of dopant incorporation for both Y (6.51%) and Gd (1.35%), as confirmed by ICP-OES measurements (see Table 1).

Figure 6a shows SEM images of the codoped samples YLa and YGd compared to a pure zirconia particle sample[27] and a 6% Y-monodoped sample[16] after heating to 1200 °C. These samples were chosen as comparison due to their comparable diameters in the ≈2 µm range. The undoped sample had sintered and displayed large grains in the micrometer range with no discernable spherical particle structures. Doping with 6% Y yielded particles still somewhat stable after heating at 1200 °C even though they had roughened surfaces and showed some particle disintegration. The destructive effects could be minimized with an optimum content of 8%–10% Y, but the particles were still comparatively rough and displayed necking.[16] La- and Gd-monodoped particles showed improved smoothness compared to Y-doped particles. At an optimum La content of 0.5%–1.0% (see Figure 2a) and Gd content of 3% (see Figure 5a), they showed an overall higher particle stability and integrity than Y-doped particles, even at their optimum content of 8%–10%. Moreover, codoping of La/Gd with Y led to the most promising results: even after heating to 1200 °C, the particles remained fully stable with relatively smooth and regular surfaces and only small grains visible on the particles' surfaces (Figure 6a). This persistency is important not only for maintaining photonic properties under operation, but also for ensuring the resuspendability of the particles prior to coating deposition and assembly.

A grain size comparison of undoped, monodoped (6% Y, 1% La, 1% Gd) and codoped (1% La/Gd with 5% Y) particles is shown in Figure 6b. At lower temperatures, grain sizes of the undoped and the 1% La/Gd-monodoped particles were similar with ≈10, ≈20 and ≈35 nm for 450, 650, and 850 °C, respectively. Smaller grain sizes were observed for all Y containing samples (YLa, YGd and 6% Y) with ≈5, ≈10 and ≈20 nm for 450, 650, and 850 °C, respectively. After heating to 1000 °C and above, this trend reversed: undoped particles displayed huge grain sizes of 860 nm after heating to 1200 °C,[27] followed by 6% Y at 180 nm, while for the codoped samples YLa and YGd, solute drag effects further attenuated the grain growth with sizes of 74 and 70 nm after 1200 °C.[16] The enhanced attenuation due to codoping compared to solely Y-monodoping was also observed for the in situ XRD measurements, as shown in Figure 3 (900 °C) and especially at higher temperatures, as shown in Supporting Information Figure S21 (1200 °C). The monodoped La/Gd samples displayed the smallest grain

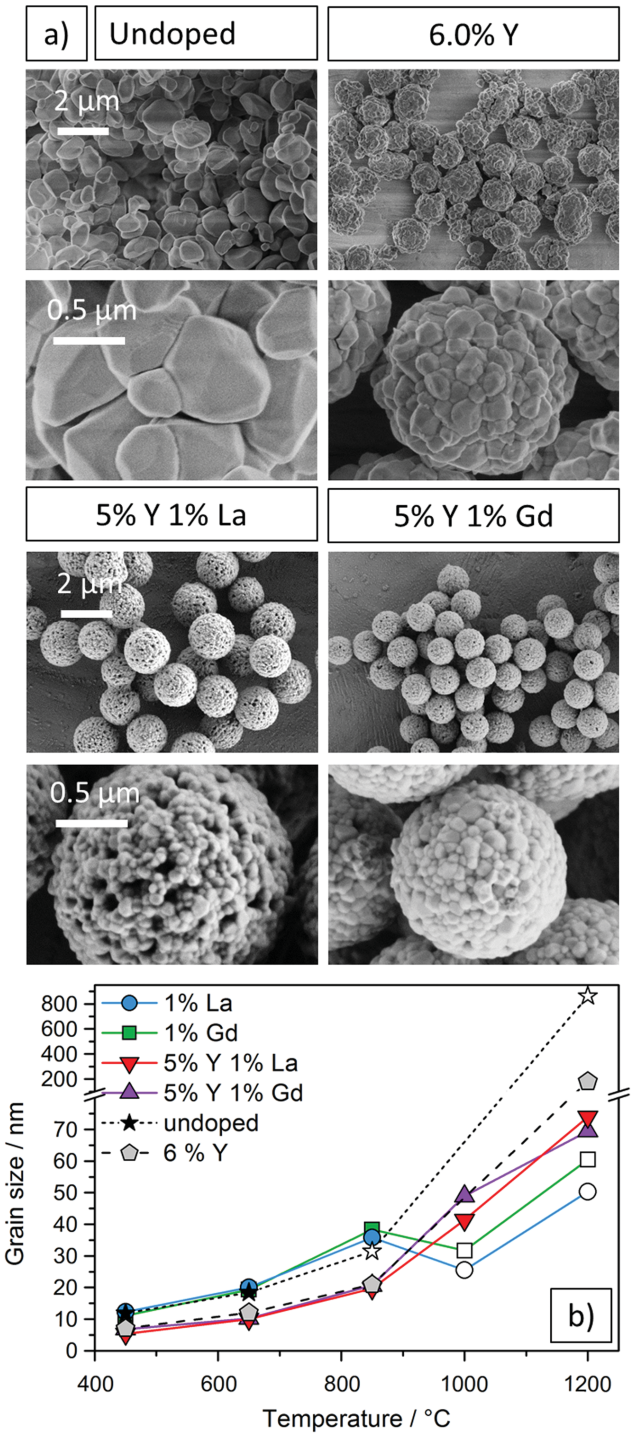

Figure 6. a) Low and high magnification SEM images of undoped zirconia particles,[27] monodoped particles with 6% Y,[16] and codoped particles with 5% Y, 1% La and 5% Y, 1% Gd. All samples shown after heating to 1200 °C. Scale bars apply to all images within a row. Samples with initial diameters in the 2 µm range were chosen for comparison. b) Comparison of grain sizes as a function of the heating temperature for monodoped samples with 1% La, 1% Gd, and 6% Y;[16] codoped samples with 5% Y, 1% La, and 5% Y, 1% Gd; and undoped zirconia particles.[27] Filled-in symbols represent the tetragonal phase, open symbols the monoclinic phase. Grain sizes <80 nm were determined via XRD (Scherrer equation), grain sizes >80 nm were determined via SEM.

© 2016 The Authors. Published by WILEY-VCH Verlag GmbH & Co. KGaA, Weinheim

sizes with 25–30 nm after heating to 1000 °C and 50–60 nm after 1200 °C. These extremely small grain sizes in the monodoped La/Gd samples coincided with a transformation from the tetragonal to the monoclinic phase, as discussed in Section 2.2. In general, the grain sizes of the La/Gd-monodoped and codoped particles were up to 130 nm and 100 nm smaller, respectively, than the grain sizes obtained for the YSZ particles. After heating at 1500 °C, codoping produced the best results with average grain sizes of 634 and 647 nm for YLa and YGd, respectively. These values were only slightly smaller than those reported for YSZ microparticles at 1500 °C (691 nm) and significantly smaller compared to those for undoped zirconia microparticles (2332 nm).[16,27]

Although monodoped La/Gd particles typically consisted of smaller grain sizes than the codoped samples YLa and YGd after heating to ≥1000 °C, the latter exhibited a higher stability and smoother surfaces after heating to 1200 °C. This can likely be explained by the tetragonal-to-monoclinic phase transformation occurring in the monodoped La/Gd particles between 850 and 1200 °C, which is accompanied by a 4% volume expansion. This expansion might push the grains apart and cause the rougher surfaces and partial disintegration observed for the La/Gd-monodoped particles. Hence, it was shown that a combination of the phase stabilizing effect of the Y ions and the grain growth attenuating effect of the La/Gd ions yielded particles with the best high-temperature stability and low size standard deviations of ≈6%–7%.

3. Conclusion

In summary, we synthesized spherical ≈2 µm zirconia particles with low size distributions and rather smooth surfaces doped with La, Gd, and a combination of La or Gd with Y. We were able to confirm the integration of the dopant ions by ICP-OES and XRD measurements. The particle stability at high temperatures was evaluated by heating them up to temperatures of 1500 °C and examining their morphology, their retained room temperature crystalline phases and grain growth. It was found that optimum La- and Gd-doping contents of 0.5%–1.0% and 3.0%, respectively, led to moderately stable particles after heating to 1200 °C, which was attributed to attenuated grain growth. However, the particles could not be stabilized in the tetragonal phase and transformed to the monoclinic phase after heating to 850–1200 °C. Furthermore, the formation of pyrochlores $La_2Zr_2O_7$ and $Gd_2Zr_2O_7$ was observed for particles doped with 3.0% La and Gd after heating to 1200 and 1500 °C, respectively. The formation of the pyrochlore phase was correlated with particle destabilization for La-doping, which was attributed to a mismatch of the thermal expansion coefficients of the pyrochlore phases with the zirconia host material. The formation of smaller monoclinic grains from larger tetragonal grains was observed upon cooling and possible mechanisms due to twinning and nucleation at a pyrochlore/La-enriched interface were proposed. Finally, codoping with 5% Y and either 1% La or 1% Gd resulted in particles that were extremely stable after heating to 1200 °C, exhibited small grain sizes, and were also stabilized in the tetragonal phase up until 1500 °C. We conclude that a combination of the phase stabilizing effects of Y-doping and the grain growth attenuation achieved through La/Gd-doping yields extremely high-temperature stable particles. While further research is required to assess their long-term performance, these particles constitute promising building blocks for the development of novel photonic coatings considered for energy systems and heat management, such as emitters/absorbers used in thermophotovoltaics[7] and reflective TBCs.[4–6]

4. Experimental Section

Materials: *n*-Butanol (99.5%) with a maximum water content of 0.1% was obtained from Th.Geyer, *n*-propanol (99.7%) from Sigma-Aldrich, ethanol (99.5%) from Grüssing, eicosanoic acid (99%) from Sigma-Aldrich, zirconium *n*-propoxide (70 wt% in *n*-propanol) from Alfa Aesar and Aldrich, yttrium *iso*-propoxide (90%) from ABCR, lanthanum *iso*-propoxide (99%) from ABCR, gadolinium *iso*-propoxide (99%) from ABCR, zeolith molecular sieve (0.4 nm) from Merck, 0.20 and 0.10 µm Minisart-Plus syringe filters 17823 from Sartorius Stedim Biotech, and demineralized water (ACS reagent grade) was obtained from Aldrich. All alkoxides were stored in a glove box.

Particle Synthesis: Zirconia particles doped with La, Gd, and Y were synthesized according to a sol–gel approach reported previously by the authors for the fabrication of pure ZrO_2 and YSZ microparticles.[16,27] The method is based on the works of Yan et al.[28,29] *n*-Butanol was dried over 0.4 nm molecular sieves and freed from dust using a syringe filter (pore size 0.20 µm). The reaction was carried out in a 250 mL wide-mouth glass bottle. The dopants were introduced to the reaction in the form of lanthanum, gadolinium, or yttrium *iso*-propoxide. Those *iso*-propoxide powders were suspended in 10 mL dry *n*-propanol, mixed with 12.2 g (26.1 mmol) zirconium *n*-propoxide (70% in *n*-propanol), and homogenized by ultrasonication. The mixture containing the zirconia and the dopant precursors was filtered through a syringe filter (pore size 0.10 µm) and added under vigorous stirring to a solution of 1.06 g (3.39 mmol) eicosanoic acid in 100 mL dried *n*-butanol at 50 °C. After 30 min, a freshly prepared solution of 1.5 mL (83.2 mmol) water in 87 mL *n*-butanol was added over the course of 60 s. After an induction time of several minutes (Supporting Information, Table S1), the slightly yellow solution turned white. The glass bottle was transferred onto an analog tube roller (SRT6 Stuart, roller size length × diameter: 340 × 30 mm^2) for an ageing time of 90 min at a rotation speed of 12 rpm. With tube diameters of 30 mm and a bottle diameter of 70 mm, this corresponded to approximately five bottle revolutions per minute. Finally, the particle suspension was poured into 200 mL of *n*-butanol at 0 °C, and the particles were separated by centrifugation (250–500 ×*g*) at 0 °C.

In order to obtain particles with different dopant contents, the amount of added lanthanum, gadolinium, or yttrium *iso*-propoxide was varied while keeping the amount of zirconium *n*-propoxide fixed. Particles with La/(La+Zr) and Gd/(Gd+Zr) molar contents of 0.5%, 1.0%, 1.5%, 2.0%, and 3.0% were obtained. Additionally, mixed dopant particles were also synthesized with molar concentrations of 1% La/(La+Y+Zr) and 5% Y/(La+Y+Zr) for La/Y particles and of 1% Gd/(Gd+Y+Zr) and 5% Y/(Gd+Y+Zr) for Gd/Y particles. The exact amounts of lanthanum, gadolinium, and yttrium *iso*-propoxide added can be found in the Supporting Information in Table S1.

Heating Experiments and Particle Characterization: The as-synthesized particles were dried at 80 °C under air for 4 h. The obtained powder samples were heated in a muffle oven (L9/SKM, Nabertherm) with a 5 °C min^{-1} heating and cooling rate and at temperatures of 250, 450, 650, 850 and 1000 °C for 3 h, with separate samples for each temperature. High-temperature anneals were performed in a tube furnace (STF 16/100, Carbolite) with a 5 °C min^{-1} heating and cooling rate and at temperatures of 1200 and 1500 °C for 3 h. The heating rate profiles are shown in Figure S1 (Supporting Information).

The crystal structure of the samples after heating was investigated by powder XRD using a Philips X'Pert PRO MPD with Cu-Kα radiation

© 2016 The Authors. Published by WILEY-VCH Verlag GmbH & Co. KGaA, Weinheim

and a Bragg–Brentano geometry. Grain sizes were calculated using the Scherrer equation with the full width at half maximum obtained from Lorentz fits of the peaks in the X-ray diffractograms using the (101) and (11-1) reflexes for the tetragonal and monoclinic structure, respectively, and a shape factor of 1. The instrumental broadening of 0.06° was taken into account, enabling estimations of the grain size up to ≈80 nm. The particle morphology and stability were assessed by scanning electron microscopy (SEM, EVO MA 10 and a Leo 1550 Gemini, both Zeiss). The particle sizes and size standard deviations were measured using SEM images by counting at least 100 particles per batch with the software ImageJ. EDX maps were measured using samples YLa and YGd.

High-energy XRD experiments with a heater apparatus developed at the Helmholtz-Zentrum Geesthacht were carried out in situ at the HEMS beamline (P07) in experimental hutch EH1 at the PETRA III synchrotron radiation source. The samples were illuminated with an X-ray beam of size up to 0.5 × 0.5 mm^2 at the sample position. The X-ray energy was 86.7 keV. A Perkin Elmer XRD 1621 detector was used to detect the scattering patterns at a sample-to-detector distance of 1162 mm.

The particle samples in the form of loose powder were put on a substrate and balanced on a ceramic sample holder. A silicon wafer was used as a substrate for temperatures up to 900 °C and platinum foil was used for experiments at 1200 °C. The sample thickness was about 1 mm in the X-ray beam direction and the sample volume was about 1 mm^3 in total. The samples were heated with two focusing infrared lamps (Osram Xenophot 64635 HLX, 150 W, 15 V, GZ6.35) with a focus size of about 1 mm^3 in air (relative humidity 24%) up to ≈900 °C. The temperature was measured using a K-type thermocouple for experiments up to 900 °C and an S-type thermocouple for 1200 °C. XRD images were gathered during the heating process with an exposure time per image of 7 s. The particles were heated to ≈900 and 1200 °C at a rate of 11 °C min^{-1}, held for 60 min and then cooled to room temperature at a rate of 11 °C min^{-1}. A heating and cooling rate of 90 °C min^{-1} was also used for samples at 1200 °C. Besides the samples La1.0 and YLa, synthesized in this study, a pure YSZ sample with a Y content of 6% from our previous study[16] was included as a comparison.

The measured scattering patterns were corrected for detector tilt and averaged over the azimuth angle using the Fit2d software developed at ESRF.[40] A quantitative analysis of the phase fractions and crystallite sizes of the monoclinic and tetragonal fractions was performed using the Maud software.[41] CeO_2 powder (NIST standard reference material SRM 674b, crystallite size $L = 380.6$ nm, $a = 0.5411651$ nm) was used as a calibration standard for the beam center, sample-to-detector distance, Caglioti parameters, and crystallite size in the Rietveld phase analysis. The CeO_2 powder was measured separately at room temperature. For very low phase fractions, the crystallite size could not be determined, even when a qualitative weight fraction of the phase was obtained.

The particle composition was analyzed by ICP-OES (Spectro Model ARCOS spectrometer). ICP-OES samples were prepared by salt fusion in a 50 wt% mixture of sodium/potassium carbonate and lithium metaborate followed by dissolution in 8% nitric acid–deionized water. Particle stability to resuspension was assessed by suspending 5–10 mg per particle sample in 5–10 drops of ethanol with a sonicator (Badelin, Sonorex Super RK 106) for at least 5 min. The sample suspensions were dropped on an aluminum stub for SEM investigations.

Supporting Information

Supporting Information is available from the Wiley Online Library or from the author.

Acknowledgements

The authors gratefully acknowledge financial support from the German Research Foundation (DFG) via SFB 986 "Tailor-Made Multi-Scale Materials Systems: M3", projects C5, C6, Z2, and A1. The authors thank Frank Meyberg and the analytics department for conducting the ICP-OES measurements, Robert Schön for HR-SEM and EDX measurements, and Almut Barck for the ex situ XRD measurements. The authors also thank Anke Puchert, Sebastian Döring, and Martin Sosniok for their contributions regarding some experimental procedures.

Received: March 5, 2016
Revised: April 26, 2016
Published online: June 13, 2016

[1] H. Uchiyama, K. Takagi, H. Kozuka, *Colloids Surf., A* **2012**, *403*, 121.
[2] I. Freris, P. Riello, F. Enrichi, D. Cristofori, A. Benedetti, *Opt. Mater.* **2011**, *33*, 1745.
[3] W. Stichert, F. Schüth, *Chem. Mater.* **1998**, *10*, 2020.
[4] D. R. Clarke, C. G. Levi, *Annu. Rev. Mater. Res.* **2003**, *33*, 383.
[5] V. Shklover, L. Braginsky, G. Witz, M. Mishrikey, C. Hafner, *J. Comput. Theor. Nanosci.* **2008**, *5*, 862.
[6] P. N. Dyachenko, J. J. do Rosário, E. W. Leib, A. Y. Petrov, R. Kubrin, G. A. Schneider, H. Weller, T. Vossmeyer, M. Eich, *ACS Photonics* **2014**, *1*, 1127.
[7] P. N. Dyachenko, J. J. do Rosário, E. W. Leib, A. Y. Petrov, M. Störmer, H. Weller, T. Vossmeyer, G. A. Schneider, M. Eich, *Opt. Express* **2015**, *23*, A1236.
[8] R. H. J. Hannink, P. M. Kelly, B. C. Muddle, *J. Am. Ceram. Soc.* **2000**, *83*, 461.
[9] S. A. Ostanin, E. I. Salamatov, *J. Exp. Theor. Phys. Lett.* **2001**, *74*, 552.
[10] K. Uchiyama, T. Ogihara, T. Ikemoto, N. Mizutani, M. Kato, *J. Mater. Sci.* **1987**, *22*, 4343.
[11] M. Keshmiri, O. Kesler, *Acta Mater.* **2006**, *54*, 4149.
[12] Z. Hua, X. M. Wang, P. Xiao, J. Shi, *J. Eur. Ceram. Soc.* **2006**, *26*, 2257.
[13] B. Aktas, S. Tekeli, S. Salman, *Adv. Mater. Lett.* **2014**, *5*, 260.
[14] X. Q. Cao, R. Vassen, W. Jungen, S. Schwartz, F. Tietz, D. Stöver, *J. Am. Ceram. Soc.* **2001**, *84*, 2086.
[15] M. J. Kelly, D. E. Wolfe, J. Singh, J. Eldridge, D.-M. Zhu, R. Miller, *Int. J. Appl. Ceram. Technol.* **2006**, *3*, 81.
[16] E. W. Leib, R. M. Pasquarelli, J. J. do Rosário, P. N. Dyachenko, S. Döring, A. Puchert, A. Y. Petrov, M. Eich, G. A. Schneider, R. Janssen, H. Weller, T. Vossmeyer, *J. Mater. Chem. C* **2016**, *4*, 62.
[17] J. A. Allemann, B. Michel, H.-B. Märki, L. J. Gauckler, E. M. Moser, *J. Eur. Ceram. Soc.* **1995**, *15*, 951.
[18] I.-W. Chen, *Mater. Sci. Eng., A* **1993**, *166*, 51.
[19] S.-L. Hwang, I.-W. Chen, *J. Am. Ceram. Soc.* **1990**, *73*, 3269.
[20] K. Jiang, S. Liu, C. Li, *J. Am. Ceram. Soc.* **2013**, *96*, 3296.
[21] B. Bastide, P. Odier, J. P. Coutures, *J. Am. Ceram. Soc.* **1988**, *71*, 449.
[22] F. H. Brown, P. Duwez, *J. Am. Ceram. Soc.* **1955**, *38*, 95.
[23] R. S. Roth, *J. Res. Natl. Bur. Stand.* **1956**, *56*, 17.
[24] A. Rouanet, *Rev. Int. Hautes Temp. Refract.* **1971**, *8*, 161.
[25] E. Bakan, D. E. Mack, G. Mauer, R. Vaßen, *J. Am. Ceram. Soc.* **2014**, *97*, 4045.
[26] R. Vaßen, M. O. Jarligo, T. Steinke, D. E. Mack, D. Stöver, *Surf. Coat. Technol.* **2010**, *205*, 938.
[27] E. W. Leib, U. Vainio, R. M. Pasquarelli, J. Kus, C. Czaschke, N. Walter, R. Janssen, M. Müller, A. Schreyer, H. Weller, T. Vossmeyer, *J. Colloid Interface Sci.* **2015**, *448*, 582.
[28] B. Yan, C. V. McNeff, F. Chen, P. W. Carr, A. V. McCormick, *J. Am. Ceram. Soc.* **2001**, *84*, 1721.
[29] B. Yan, C. V. McNeff, P. W. Carr, A. V. McCormick, *J. Am. Ceram. Soc.* **2005**, *88*, 707.
[30] R. D. Shannon, *Acta Cryst.* **1976**, *A32*, 751.
[31] G. I. Spijksma, *Doctoral Dissertation*, Universiteit Twente, The Netherlands, **2006**.

© 2016 The Authors. Published by WILEY-VCH Verlag GmbH & Co. KGaA, Weinheim

[32] D. Bradley, R. C. Mehrotra, I. Rothwell, A. Singh, *Alkoxo and Aryloxo Derivates of Metals*, Academic Press, London **2001**.
[33] V. P. Dravid, M. R. Notis, C. E. Lyman, *J. Am. Ceram. Soc.* **1988**, *71*, C219.
[34] Y.-C. Wu, Y.-T. Chiang, *J. Am. Ceram. Soc.* **2011**, *94*, 2200.
[35] A. H. Heuer, M. Rühle, *Acta Metall.* **1985**, *33*, 2101.
[36] J. E. Bailey, *Proc. R. Soc. Lond. A* **1964**, *279*, 395.
[37] X. Z. Wang, X. Y. Liu, A. Javed, C. Zhu, G. Y. Liang, *J. Mol. Liq.* **2015**, *207*, 309.
[38] H. Lehmann, D. Pitzer, G. Pracht, R. Vassen, D. Stöver, *J. Am. Ceram. Soc.* **2003**, *86*, 1338.
[39] M. Li, Z. Feng, P. Ying, Q. Xin, C. Li, *Phys. Chem. Chem. Phys.* **2003**, *5*, 5326.
[40] A. P. Hammersley, S. O. Svensson, M. Hanfland, A. N. Fitch, D. Hausermann, *High Pressure Res.* **1996**, *14*, 235.
[41] L. Lutterotti, S. Matthies, H.-R. Wenk, A. S. Schultz, J. W. Richardson, *J. Appl. Phys.* **1997**, *81*, 594.

© 2016 The Authors. Published by WILEY-VCH Verlag GmbH & Co. KGaA, Weinheim